Mining, Metallurgy & Exploration (2022) 39:1841–1851
https://doi.org/10.1007/s42461-022-00613-0

Pressure-Quantity Characteristic Curves for a Mature Panel Cave

R. Bhargava[1] · P. Tukkaraja[1] · S. Jayaraman Sridharan[1] · Y. Pan[1] · V. V. S. Vytla[2]

Received: 7 February 2022 / Accepted: 3 May 2022 / Published online: 17 May 2022

Abstract
Panel caving is an underground bulk mining method that utilizes gravitational force for mining massive, steeply dipping, and deep-seated ore deposits at a lower operating cost. To control dust and gas emissions entering the production level during the extraction of ore from the draw points in a panel cave, relatively negative pressure is created in the cave by installing an exhaust fan in the exhaust drift located on top of the cave. Since caving is a dynamic process, the design of an effective ventilation system is a challenging task, and therefore, estimation of airflow resistance offered by the broken rock inside the cave is critical. The complex and dynamic nature of caving also makes it difficult to predict the airflow resistance by using traditional approaches. This study investigates the effect of changes in the bulk porosity of the broken rock on the cave airflow resistance using computational fluid dynamics (CFD) approach. The results show an inverse relationship between the cave airflow resistance and the bulk cave porosity. The pressure-quantity characteristic curves presented in this paper provide valuable information for sizing and operating an exhaust fan used for a mature panel cave ventilation.

Keywords Porosity · Cave airflow resistance · Panel/block cave mining · Flow through porous media

1 Introduction

Mass mining methods such as panel caving tend to be an ideal choice for massive, steeply dipping, and deep-seated ore deposits with an ability to extract deposits at high production rates and low operating costs. The deposits mined by the caving mining method are generally disseminated or low grade in nature [1]. Previous studies reported the advantage of the panel caving mining method in terms of the maximization of net present value for low-grade ore deposits [2]. Thus, the economics for a low-grade ore deposit also tend to tilt in favor of panel caving. An optimally designed panel cave mining method can have the lowest operating cost compared to other underground mining methods subject to keeping ore dilution under checked limits [3, 4]. Super caves have been defined as those underground cave mines with a production rate exceeding 25Mt per annum or approximately 70kt/day [5, 6]. The evolution of production rates over the years for conventional and super caves is shown in Fig. 1.

The increased popularity of cave mining methods demands a robust ventilation system to support the high production rates of the future super caves. Therefore, this research study contributes to the knowledge base of panel cave mine ventilation. This study investigates a less explored concept of cave airflow resistance that plays a vital role in sizing and operating the exhaust fan used for ventilating a mature panel cave in terms of airflow and pressure requirements with respect to the cave size and caved material properties (bulk porosity).

2 Literature Review

In panel caving, the cave is assumed to be fully developed when the broken rock reaches the economic ore boundary. The airflow resistance of a cave is defined as the resistance offered by the broken rock pile to the airflow when air flows through the rock pile inside the cave. The porosity of the rockpile is defined as the percentage of air/void space inside the total volume occupied by the rock pile. The porosity of a cave varies as the cave propagates; it plays an important role in buffering an air blast event. Thus, porosity and the broken rock resistance are important parameters for modeling airflow inside the cave [7]. The leakage of airflow into

✉ P. Tukkaraja
PT@sdsmt.edu

[1] South Dakota Mines, Rapid City, SD 57701, USA

[2] MSC Software, Irvine, CA 92617, USA

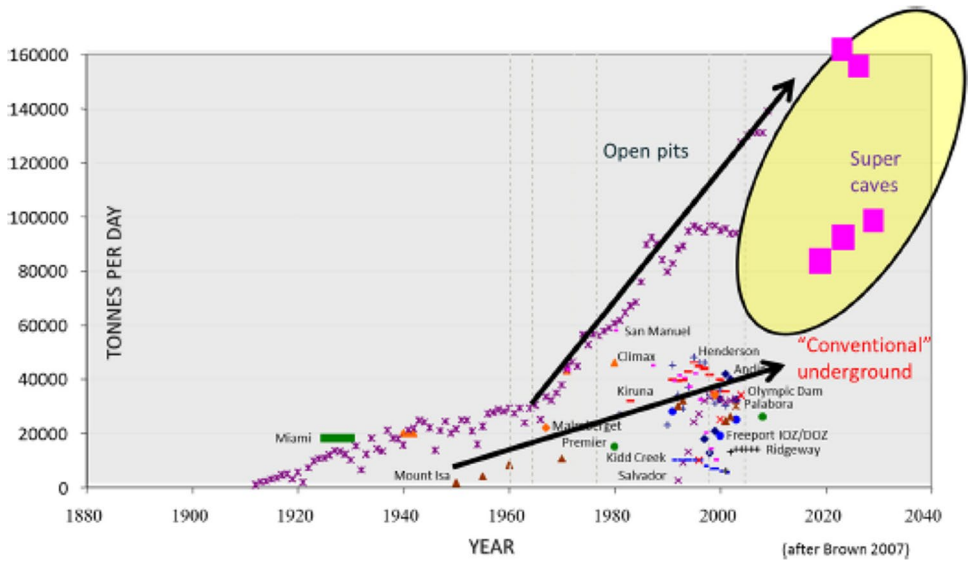

Fig. 1 Production rates: open pits, conventional underground mining, and super caves [5, 6]

the cave and ore passes from the production drifts is also an important phenomenon; it has been observed that around 40 percent of air supplied into the production drifts leaks into the cave, and the ore passes, so the production drift airflow quantity should be adjusted for accounting these leakages [8].

Several studies have been conducted to characterize airflow through broken rock [9, 10]. Porous media can be modeled as a discrete or continuum model. Discrete modeling offers certain advantages over the continuum model in terms of accuracy and realistic approach, but the meshing of the geometry becomes a tedious task in discrete modeling. The advantage of the continuum model is that it is computationally inexpensive, but accuracy gets sacrificed in the process [11]. The advantage of CFD models is to simulate fluid flows through complex scenarios where experimental and field experiments are difficult to conduct. CFD modeling has been successfully used in the past for underground mining applications involving pressure and shock losses in the ventilation configurations [12–17], radon control measures in block cave mines [18–22], the gob characteristics for a longwall gob involving spontaneous combustion [23], and airflow patterns in the room and pillar mining [24].

In a multi-lift caving operation, the older working areas might be connected to a mature cave [11]. Attempts for predicting the airflow resistance of a mature panel cave have also been made in the past with limited success. The previous study did not consider the connection of the cave to the older workings which was very unlikely for a mature cave although the study indicated that the flow inside the cave was neither laminar nor turbulent [11]. Recent scale model studies of panel cave mines help validate the CFD simulation results and use CFD to investigate the airflow distribution in the panel cave mine [25, 26].

3 Model Layout and Research Approach

This study considered a panel cave continuum model with a cave dimension of 375 m × 256 m × 356 m (height × length × width) and nine production drifts, three undercut inlet ducts, eight undercut drifts, and eight exhaust drifts. The model also contained 94 drawbells, broken rock region, and uncaved in situ rock inside the cave. These regions were simulated as porous zones. The isometric, side, and front views of the panel cave model are shown in Figs. 2 and 3. The cave advancement direction was assumed to be from right to left. Each of the production drifts, undercut drifts, and exhaust drifts have dimensions of 4.3 m × 4.3 m. There were three undercut inlet ducts (inside the undercut

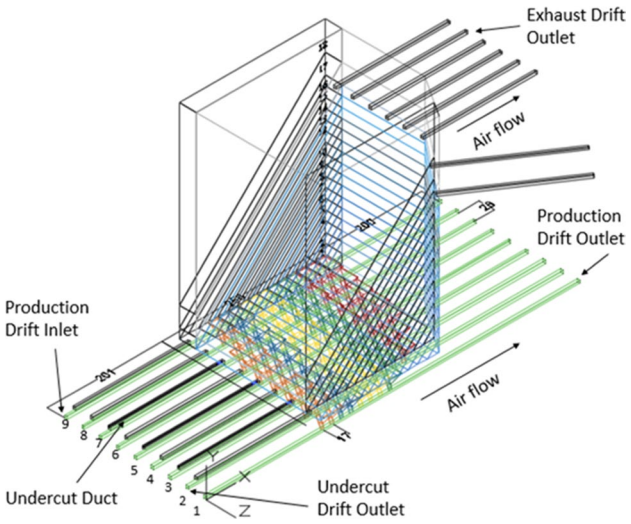

Fig. 2 Isometric view of the panel cave model [27]

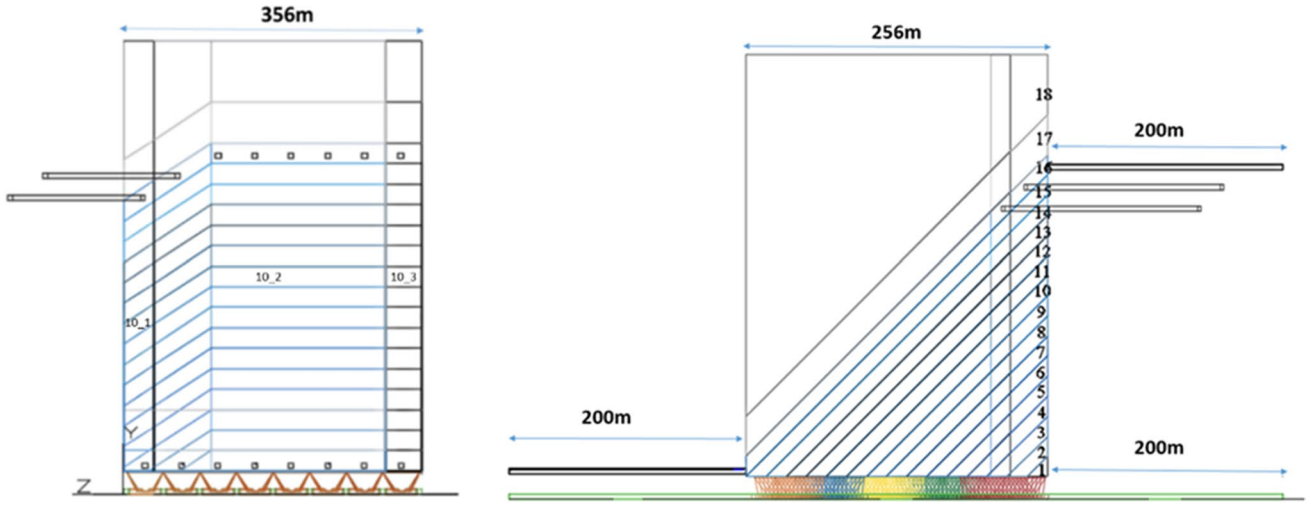

Fig. 3 Side and front views of the panel cave model [27]

drifts) of size 1 m × 1 m and were used for ventilating undercut drifts. The computational time has been kept in mind while modeling the airflow through cave zones. Therefore, broken rock zones and in situ waste rock zones were modeled diagonally, consisting of 16 broken rock zones and 2 uncaved in situ waste rock zones. Each broken rock zone was divided into 3 subregions laterally to conform to the observation in the field that the boundary of the cave had higher porosity values with larger particle sizes as compared to the mid-region. Subregions for broken rock zone 10 are shown as an example in Fig. 3. The bulk cave porosity was calculated by dividing the sum of the porous volume of broken rock from all the regions by the total volume of the cave (excluding the intact rock zone).

This study modeled broken rock zones as permeable porous media. The methodology used for this study is shown in Fig. 4. Different scenarios of cave resistance were simulated by changing cave porosity values in the model, and the pressure loss (the pressure difference was measured across the cave) obtained from the CFD analysis was plotted against airflow to obtain the equation for airflow resistance under different porosity conditions. Figure 5 shows the schematic of air leaking into the cave while all the outlets except the exhaust outlet were closed to calculate the airflow resistance by allowing the air to leak through the porous media of broken rock. This study did not consider the undercuts for calculating the airflow resistance as their effect would be minimal for a mature panel cave. It was assumed that the matured cave was connected to old workings through the exhaust drifts, as shown in Fig. 5.

A reliable result from the CFD model is highly dependent on the boundary conditions applied to the model. A summary of boundary conditions applied to the panel cave model is presented in Table 1. Static pressure condition was

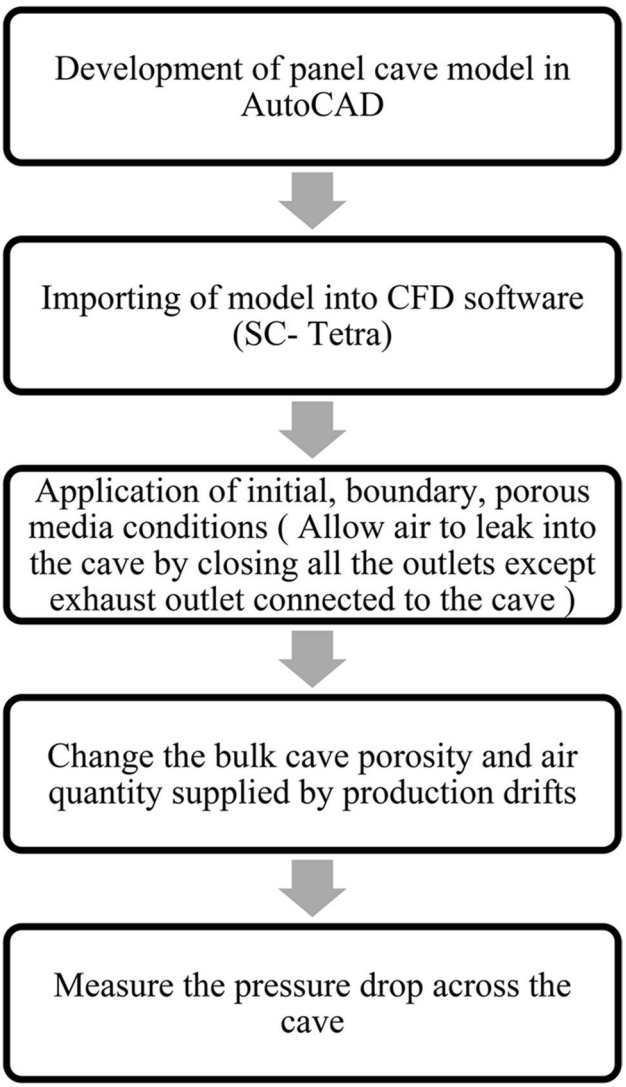

Fig. 4 Airflow resistance calculation methodology

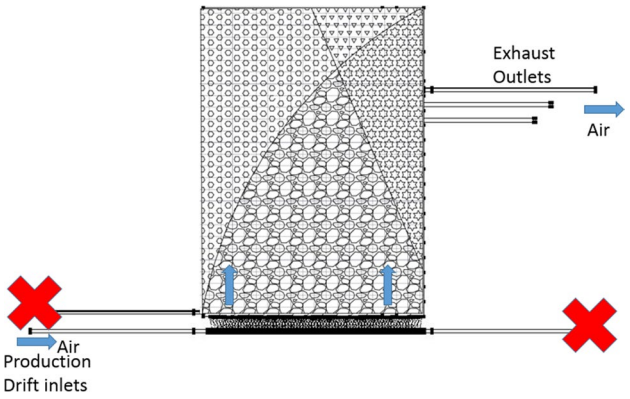

Fig. 5 Schematic illustration of air leakage into the cave

applied to the exhaust drift outlet. Natural inflow/outflow condition was used for the cave roof. This condition assumes that velocity and pressure do not change in the normal direction. It is used because the flow was assumed to continue into other sections of the mine [28].

SC/Tetra (CFD software program) consists of three sets of programs. These include the pre-processor (for creation of computational mesh and setting up the boundary conditions for the simulation), solver (for the execution of analysis), and post-processor (for visualization and analysis of the results). The simulation study considered a steady-state incompressible and turbulent airflow through the panel cave model. Standard k-ε turbulence model was used for the study to consider the effects of turbulence [12]. The flow field can be obtained by solving momentum and mass conservation equations. Therefore, for obtaining velocity and pressure fields, momentum and mass conservation equations were solved, respectively. A porous media condition was also used to consider the pressure drop of flow through the broken rock [29].

For obtaining reliable results from the CFD simulations, it is also important that the simulation results are grid-independent. A mesh independence study was also conducted for the mature panel cave model. From the analysis of the results with mesh elements ranging from 5.5 to 15.8 million, it was observed that a further increase in the mesh elements from 11.83 million did not have a significant effect on the results. Hence, 11.83 million mesh elements were used for this study.

4 Results and Discussion

4.1 CFD Simulation of the Mature Panel Cave

To calculate the broken rock airflow resistance, the mature panel cave model was analyzed under six different bulk cave porosities and five different air quantities through the production drift [30]. Figure 6 shows the measurement locations for airflow pressure at the entry of the cave (inside the production drifts) and at the exit of the cave (inside the exhaust drifts) for cave porosities of 35% and 56%, with an airflow rate of 291 m^3/s in the production drifts.

For a given porosity of the cave and airflow in the production drifts, the pressure difference across the cave was calculated and then plotted against the airflow quantity flowing through the cave, as shown in Fig. 7. For example, for a bulk cave porosity of 35%, five different air quantities were simulated. Therefore, for six different bulk cave porosities, a total of 30 simulations were performed to develop the pressure-quantity (P-Q) characteristic curves for a mature panel cave mine. Figure 8 shows the variation of the airflow resistance value with respect to the bulk cave porosity; these values are provided in Table 2.

From Fig. 7, the relationship between the pressure difference, P (Pa) across the cave, the airflow resistance, R ($Ns^{1.8}/m^{7.4}$), and the air quantity supplied, Q (m^3/s) can be summarized by

$$\Delta P = RQ^{1.8} \tag{1}$$

Equation 1 suggests that the flow inside the cave is neither fully laminar nor fully turbulent.

To validate the CFD framework used for the full-scale mature panel cave discussed in Section 4.1, we conducted a CFD simulation study for a reduced cave model (1:100). For the CFD analysis, a 1:100 reduced cave model of dimensions

Table 1 Boundary conditions

Region	Boundary condition type	Value/condition
Production drifts (9 nos.)	Fixed velocity	0.75 m/s, 1 m/s, 1.25 m/s, 1.5 m/s, and 1.75 m/s
Undercut inlet drift duct (3 nos.)	Wall condition	n/a
Undercut drift (8 nos.)	Wall condition	n/a
Exhaust drift (8 nos.)	Static pressure	Zero Pa
Cave roof	Outlet	Natural inflow/outflow

n/a not applicable

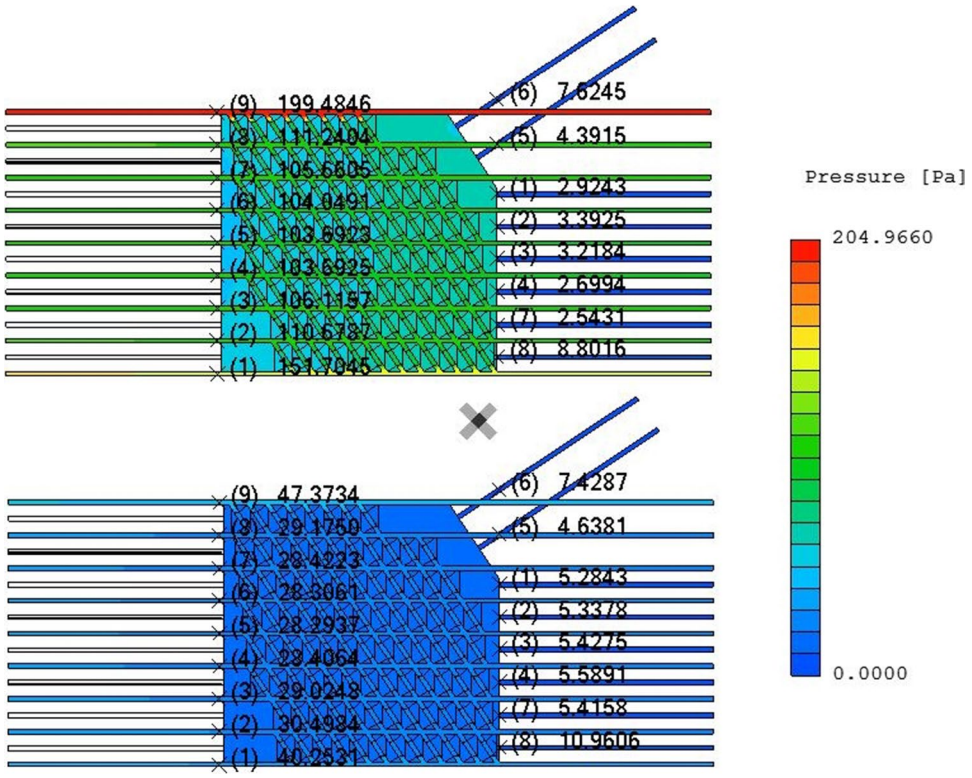

Fig. 6 Pressure measurement at entry and exit of the cave in the production and exhaust drifts at 35% and 56% cave porosity conditions (top to bottom)

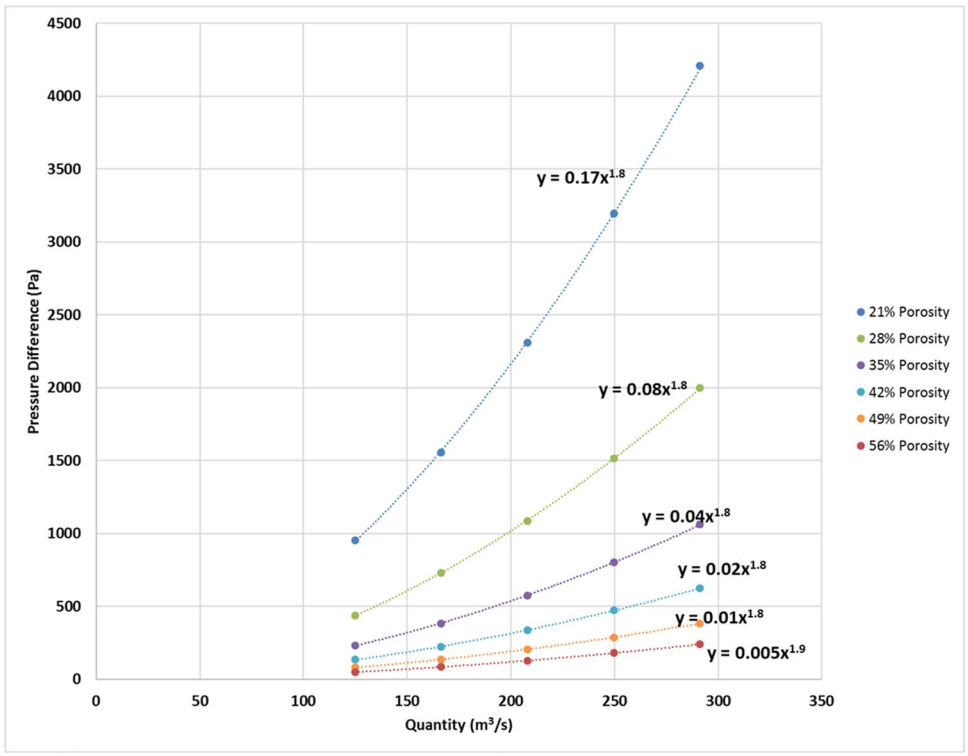

Fig. 7 Pressure-quantity characteristic curves

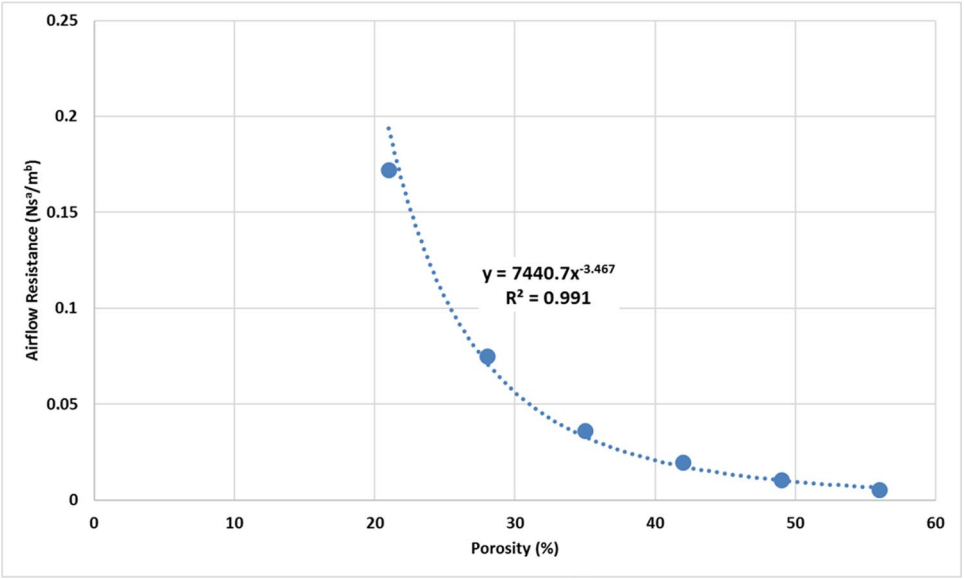

Fig. 8 Airflow resistance vs. bulk cave porosity

Table 2 Cave porosity and airflow resistance

Cave porosity (%)	Cave airflow resistance (Ns^a/m^b)
21	0.17
28	0.08
35	0.04
42	0.02
49	0.01
56	0.005

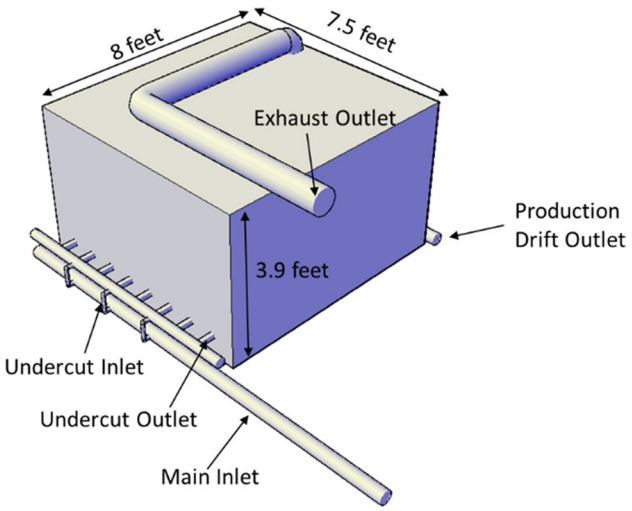

Fig. 9 Isometric view of the reduced cave model

8 ft × 7.5 ft × 3.9 ft was considered to study the effect of varying cave porosity on the pressure drop across the cave.

4.2 CFD Simulation of a Reduced Cave Model

The model consisted of 9 production drifts (1.5″ diameter), 8 undercut outlet drifts (1.5″ diameter), 3 undercut inlet drifts (0.82″ diameter), and 94 drawbells arranged in the El Teniente layout as shown in Figs. 9 and 10.

The relationship between the pressure and quantity under different bulk cave porosities (30–70%) was examined using the scaled model. For the scaled experimental model, the pressure measurements across the cave are illustrated in Figs. 11 and 12 for cave porosities of 30% and 70%, respectively.

The model was also tested for observing the pressure drop and velocity vectors under forcing and exhaust conditions, but no significant difference was observed. Figures 13 and 14 show the pressure contours and velocity vectors for the 30% porous experimental cave model for forcing and exhaust scenarios, respectively.

The *P*-*Q* characteristics curves were developed for different porosities as shown in Fig. 15 whereas the airflow resistance variation with porosity is shown in Fig. 16.

As it can be seen from Figs. 15 and 16, once the porosity of the cave approaches 50%, the cave airflow resistance does not change significantly.

4.3 Experimental Study

A reduced physical cave model representing the CFD model discussed in Section 4.2 is shown in Fig. 17. This experimental study investigated the effects of material size combinations, fan configurations, and undercut structure on the cave airflow resistance.

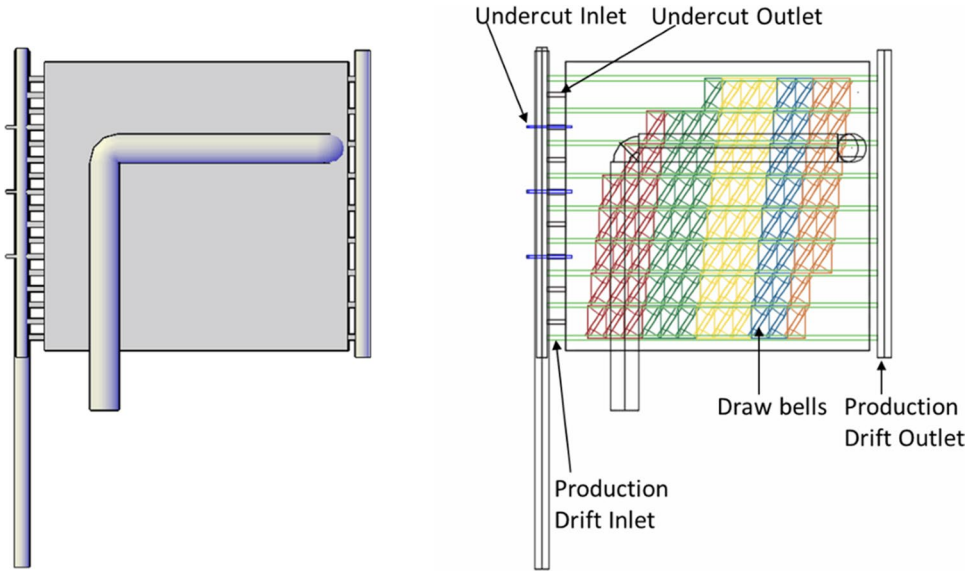

Fig. 10 Top view of the reduced cave model

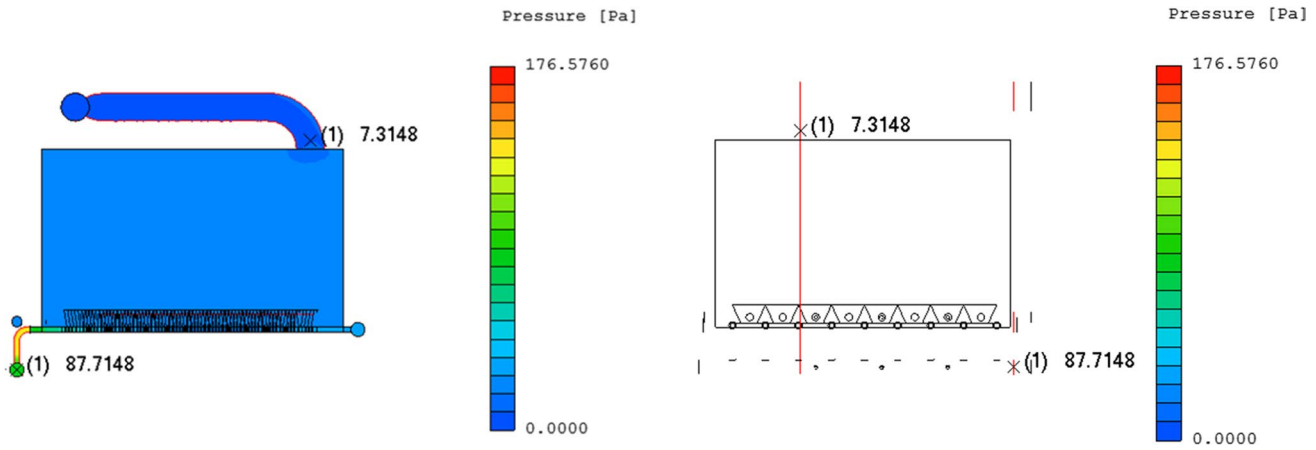

Fig. 11 Pressure measurement across the cave with 30% porosity

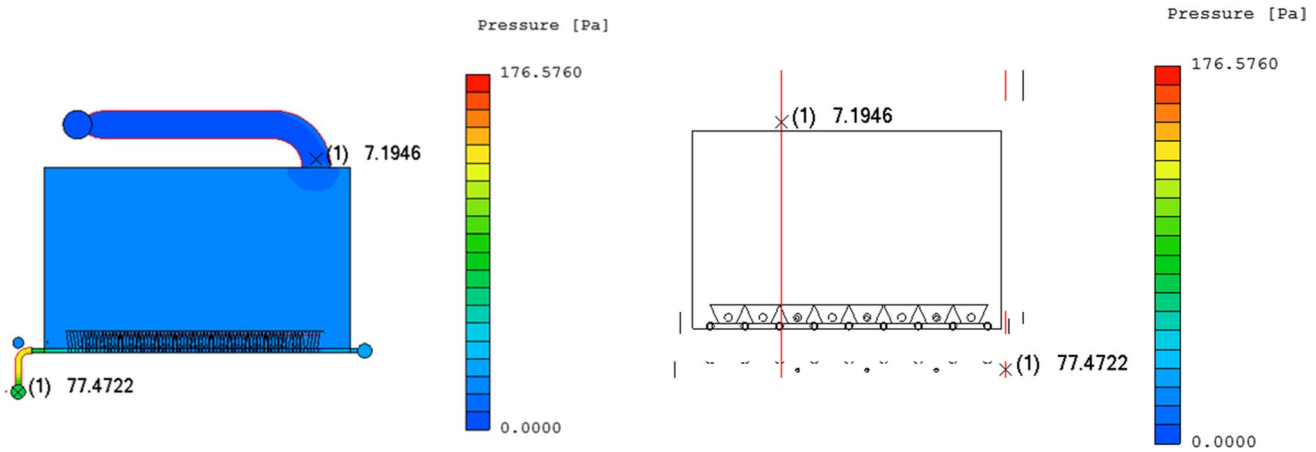

Fig. 12 Pressure measurement across the cave with 70% porosity

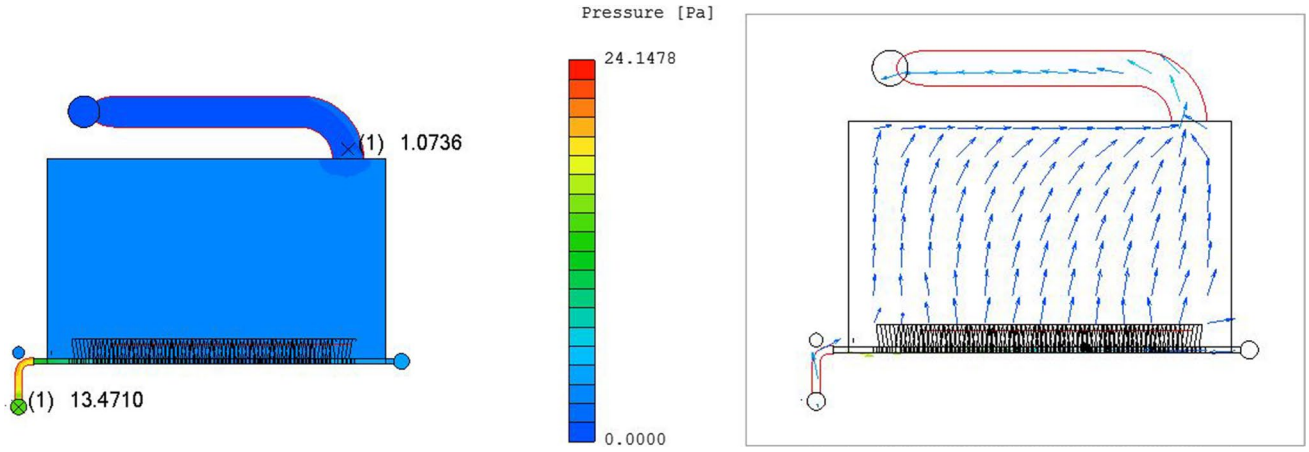

Fig. 13 Forcing system—pressure contours and velocity vectors

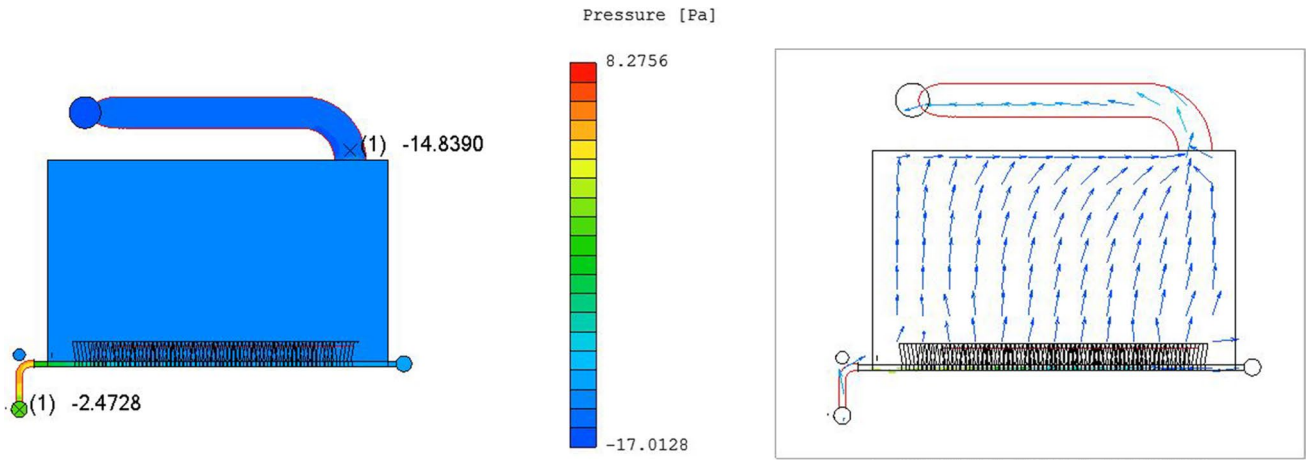

Fig. 14 Exhaust system—pressure contours and velocity vectors

In the physical scale model (1:100), the broken rock materials were not scaled down as it was difficult to achieve desired porosity values with the representative particle sizes. We simulated three porosity conditions (10%, 20%, and 16%) in the cave zone using cubic cardboard boxes of different sizes. We used 3 layers of 10 cm cubic boxes to simulate the 10% porosity condition in case 1, 2 layers of 15 cm cubic boxes to simulate the 20% porosity condition in case 2, and the 16% porosity condition was simulated using the combination of 10 cm and 15 cm boxes in case 3. Figure 18 shows the two layers of 15 cm boxes used in case 2 and the overview of the experimental setup for case 2.

To study the effect of cave porosity and particle size on the cave airflow characteristics, experiments were performed under the following conditions: four different flow conditions for the top fan with a fully open bottom fan; two undercut structure conditions (open and close). A total of 24 data sets were collected (3 cases × 4 flow conditions × 2 undercut structures = 24 experiments). Each data set was repeated to obtain two replications, and the average value was used for data analysis.

From the reduced CFD cave model simulations and experimental analyses discussed in Sections 4.2 and 4.3, respectively, it was concluded that the reduction in porosity and particle size of caved materials increased cave airflow resistance while the existing undercut openings decreased the airflow rate through production drifts, increased the overall airflow through the cave system, reduced the overall cave resistance, and increased the exponent n value in the *P*-*Q* equation. The additional fan increased cave airflow resistance and decreased the exponent *n* value [26]. Similar trends were observed in the *P*-*Q* characteristic curves developed from simulation models and physical experiments as shown in Figs. 15 and 19 respectively.

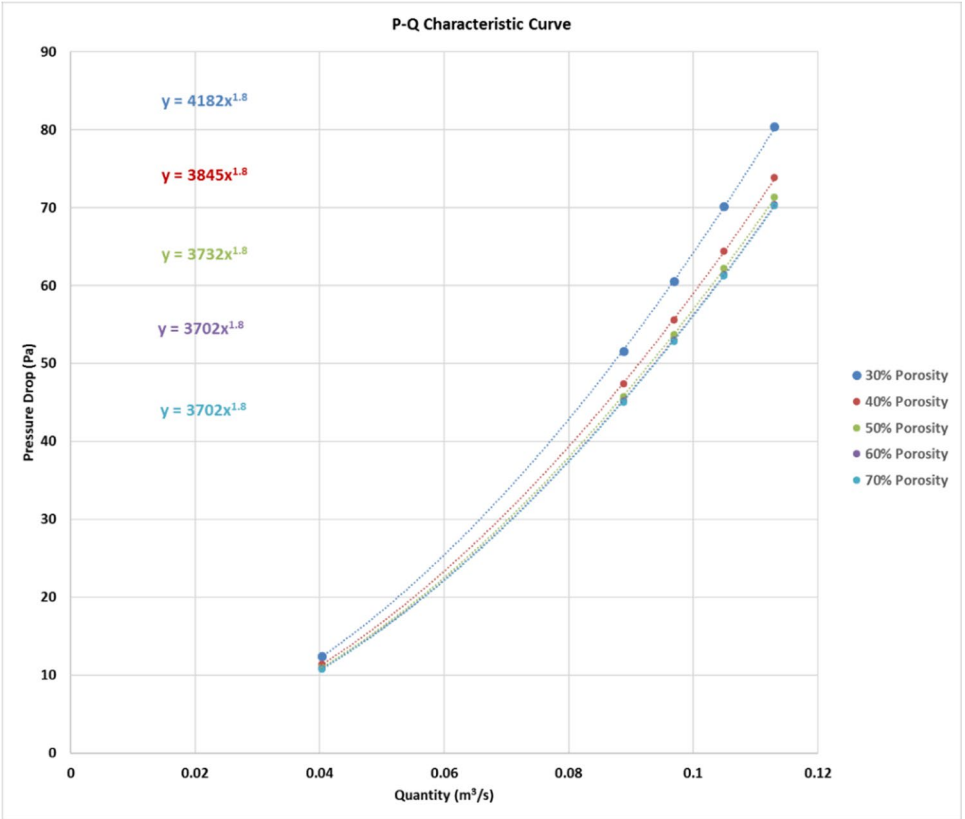

Fig. 15 Pressure-quantity characteristic curves for the reduced cave model

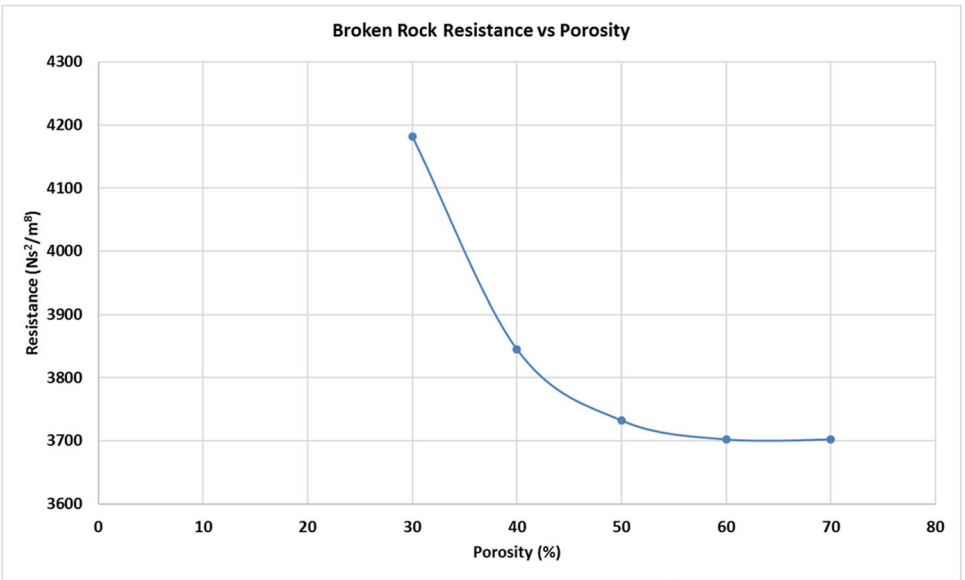

Fig. 16 Airflow resistance vs. bulk cave porosity for reduced cave model

5 Conclusions

The scope of work for this paper is to develop pressure-quantity characteristic curves for a mature panel cave. The novelty of the paper is the investigation of the panel cave mine ventilation under various cave conditions. This study is valid for a mature panel cave (with no air gap) where the cave is connected to the older working areas, or an exhaust drift located on top of the cave.

The airflow characteristics of a panel cave are examined with the help of CFD using a continuum approach. This study reveals that porosity plays a vital role in changing the resistance offered by the broken rock to the airflow leaking

Fig. 17 Flow Inlets - Nine production drifts and three undercut drifts (top); arrangement of drawbells and drawpoints with an El Teniente layout (bottom)

Fig. 18 Two layers of 15 cm boxes used in case 2 (left); overview of the cave model and fan setup (right)

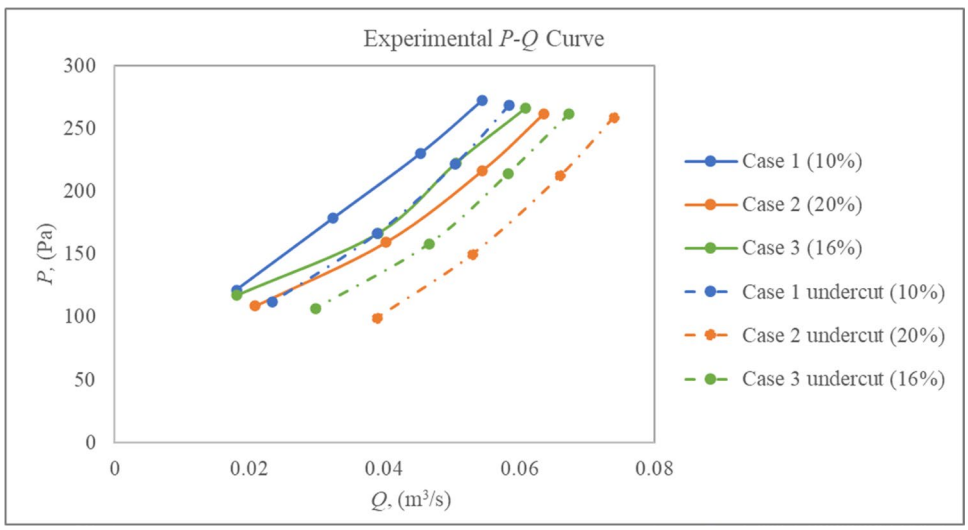

Fig. 19 *P-Q* curves for the experimental cave model under various porosity conditions (10%, 20%, and 16%) and undercut structures

into the cave. The airflow resistance increases as the porosity of the broken rock pile decreases. The resistance of the panel cave changes dynamically with the bulk porosity of the broken rock. The CFD analysis of the scaled experimental model provided valuable information critical for the success of the experimental studies. No significant change in the airflow resistance of the cave was observed beyond the upper limit of 50% cave porosity.

Funding The authors received financial support from the National Institute for Occupational Safety and Health (NIOSH) (200–2014-59613) for conducting this research.

Declarations

Conflict of Interest The authors declare no competing interests.

References

1. Lovejoy C (2012) Block caving: keeping up with caving. Min Mag 6:46–64
2. Lei Q et al (2014) Effects of geomechanical changes on the validity of a discrete fracture network representation of a realistic two-dimensional fractured rock. Int J Rock Mech Min Sci 70:507–523
3. Laubscher D (1994) Cave mining-the state of the art. J South Afr Inst Min Metall 94(10):279–293
4. Trueman R, Castro R, Halim A (2008) Study of multiple draw-zone interaction in block caving mines by means of a large 3D physical model. Int J Rock Mech Min Sci 45(7):1044–1051
5. Brown ET (2007) Block caving geomechanics: International Caving Study 1997-2004: Julius Kruttschnitt Mineral Research Centre. The University of Queensland
6. deWolfe C, Ross I (2016) Super caves - benefits, considerations and risks. in Proceedings of the 7th International conference and exhibition on mass mining, Sydney
7. Vejrazka C, Carr C, Chitombo G (2016) Northparkes mines' current air blast risk assessment practices for block caving operations. Proceedings of MassMin 2016:257–264
8. Brokering RD, Loring DM, Rutter CJ (2017) Practical implementation of VOD at the Henderson mine. In Proceeding of the 16th North American Mine Ventilation Symposium, pp 17–22
9. Schafrik S (2015) The use of packed sphere modelling for airflow and heat exchange analysis in broken or fragmented rock (Doctoral dissertation, Laurentian University of Sudbury)
10. Schafrik S, Millar DL (2015) Verification of a CFD code use for air flow simulations of fractured and broken rock. Appl Therm Eng 90:1131–1143
11. Baysal A, Ajayi KM, Tukkaraja P, Shahbazi K, Katzenstein K, Loring D (2017) Prediction of airflow resistance of a mature panel cave. In 16th North American Mine Ventilation Symposium 14:27–34
12. Hurtado JP et al (2014) Shock losses characterization of ventilation circuits for block caving production levels. Tunn Undergr Space Technol 41:88–94
13. Sridharan SJ, Sastry BS (2020) New prediction models for estimation of aerodynamic pressure loss due to a train of mine cars in an underground airway. Mining Metall Explor 37(5):1571–1582
14. Purushotham T, Sastry BS, Samanta B (2010) Estimation of shock loss factors at shaft bottom junction using computational fluid dynamics and scale model studies. CIM J, p. Medium: X; Size: page(s) 130–139
15. Ajayi KM et al (2019) Prediction of airway resistance in panel cave mines using a discrete and continuum model. Int J Min Sci Technol 29(5):781–784
16. Tukkaraja P, Bandopadhyay S (2010) Analyzing shock losses at air-crossings in a mine ventilation network using CFD simulations. Conference: The 13. U.S./North American mine ventilation symposium, Sudbury, ON (Canada), 13–16 June 2010
17. Purushotham T, Bandopadhyay S (2009) Estimation of shock loss coefficient values of mine ventilation configurations using CFD simulations. in Proceedings of 9th International Mine Ventialtion Congress
18. Tukkaraja P, Bhargava R, Jayaraman Sridharan S (2021) Radon in underground mines, in Mining Technology. https://doi.org/10.5772/intechopen.101247
19. Ajayi K et al (2019) Numerical investigation of the effectiveness of radon control measures in cave mines. Int J Min Sci Technol 29(3):469–475
20. Ajayi KM et al (2019) Estimation of radon diffusivity tensor for fractured rocks in cave mines using a discrete fracture network model. J Environ Radioact 196:104–112
21 Bhargava R et al (2019) CFD analysis of the effect of porosity, quantity and emanating power variation on gas emissions in block/panel cave mines. Springer Singapore, Singapore
22. Ajayi KM et al (2018) A discrete model for prediction of radon flux from fractured rocks. J Rock Mech Geotech Eng 10(5):879–892
23. Yuan L, Smith A (2008) Effects of ventilation and gob characteristics on spontaneous heating in longwall gob areas. in of: Proceedings of the 12th US/North American Mine Ventilation Symposium
24. MitevRanjan KK, Ghosh SK (2013) Mine ventilation in a board and pillar mines using CFD. Int J Emerging Technol Adv Eng 3(3):389–393
25. Jha A et al (2021) Scale model investigation of ventilation parameters in a block cave mine. CRC Press, London, pp 556–562
26. Pan Y et al (2021) Investigation of airflow characteristics under parallel fan conditions in a block cave mine. CIM J 12(4):169–178
27. Bhargava R, Tukkaraja P, Shahbazi K, Katzenstein K, Loring D (2019) CFD analysis of the effect of porosity, quantity and emanating power variation on gas emissions in block/panel cave mines. In Proceedings of the 11th International Mine Ventilation Congress. Springer, Singapore, pp 838–849
28. Ajayi K et al (2015) Computational fluid dynamics study of radon gas migration in a block caving mine. 15th North American Mine Ventilation Symposium. Virginia Tech, Department of Mining and Minerals Engineering 341–348
29. Cradle (2015) User's guide : basics of CFD analysis
30. Bhargava R et al (2021) Airflow characteristic curves for a mature block cave mine. CRC Press, London, pp 56–64